

Higher-Order Moment-Method Modeling of Curved Metallic Antennas and Scatterers

Miroslav Djordjević* and Branislav M. Notaroš

University of Massachusetts Dartmouth, ECE Department
285 Old Westport Road, North Dartmouth, MA 02747, bnotaros@umassd.edu

1. Introduction

Higher-order (large-domain) basis functions for the approximation of electric surface currents over electrically large bilinear quadrilateral surface elements (patches) [1] have significant computational advantages over traditionally used low-order (small-domain) basis functions in the method of moments (MoM) analysis of metallic antennas and scatterers. However, a major problem with these basis functions is their relative inefficiency at modeling of surfaces with pronounced curvature because many small patches may be required for the geometrical precision of the model, and then higher-order basis functions actually reduce to low-order functions (on small patches).

In order to overcome this deficiency, we propose a MoM technique using generalized curved parametric quadrilaterals of arbitrary geometrical order. In the new technique, the geometrical surface elements in the model can be both electrically large, with higher-order basis functions for current modeling, and curved. With this, the large-domain current-modeling efficiency is preserved even for surfaces with pronounced curvature (such as a sphere or a cylinder). The geometrical orders of the quadrilateral elements are entirely independent from the current-approximation orders of the basis functions, and the two sets of parameters of the higher-order model can be adopted at will for the best overall performance of the method. Numerical examples showing the efficiency and accuracy of the new technique are a metallic spherical scatterer, analyzed using four different higher-order models, and an antenna system consisting of two wire monopoles attached to a metallic cylinder.

2. Geometrical Modeling and Current Expansion

As basic elements for geometrical modeling of metallic antennas and scatterers, we use generalized curved parametric quadrilaterals of higher (arbitrary) geometrical orders (Fig.1). A generalized quadrilateral is determined by $M=(K_u+1)(K_v+1)$ points (interpolation nodes) arbitrarily positioned in space, where K_u and K_v ($K_u, K_v \geq 1$) are geometrical orders of the element along u - and v - parametric coordinates, respectively. It can be described analytically as

$$\mathbf{r}(u, v) = \sum_{m=1}^M \mathbf{r}_m p_m(u, v) = \sum_{i=0}^{K_u} \sum_{j=0}^{K_v} \mathbf{r}_{ij} u^i v^j, \quad -1 \leq u, v \leq 1, \quad (1)$$

where $\mathbf{r}_1, \mathbf{r}_2, \dots, \mathbf{r}_M$ are the position vectors of the interpolation nodes, $p_m(u, v)$ are

This work was supported by the National Science Foundation under grant ECS-0115756.

Lagrange-type interpolation polynomials satisfying the Kronecker delta relation $p_j(u_j, v_j) = \delta_{ij}$, with u_j and v_j being the parametric coordinates of the j -th node, and \mathbf{r}_{ij} are constant vector coefficients related to $\mathbf{r}_1, \mathbf{r}_2, \dots, \mathbf{r}_M$. The simplest element (defined by $K_u = K_v = 1$), called the bilinear quadrilateral and shown in Fig.2, is determined by its four ($M=4$) vertices that can be arbitrarily positioned in space [1]. Its edges and all parametric lines are straight. Of course, geometrically higher-order quadrilateral elements ($K_u, K_v > 1$) allow better flexibility and accuracy in modeling of complex curved structures. However, the use of flexible higher-order curved elements is cost effective only if they can be made electrically large, which implies the use of higher-order current expansions within the elements as well.

The surface electric current density vector over quadrilaterals is represented as

$$\mathbf{J}_S(u, v) = \frac{1}{W(u, v)} \left(\sum_{i=0}^{N_u} \sum_{j=0}^{N_v-1} \alpha_{uj} f_{uj}(u, v) \mathbf{a}_u(u, v) + \sum_{i=0}^{N_u-1} \sum_{j=0}^{N_v} \alpha_{vij} f_{vij}(u, v) \mathbf{a}_v(u, v) \right), \quad (2)$$

$$W(u, v) = |\mathbf{a}_u(u, v) \times \mathbf{a}_v(u, v)|, \quad \mathbf{a}_u(u, v) = \frac{\partial \mathbf{r}(u, v)}{\partial u}, \quad \mathbf{a}_v(u, v) = \frac{\partial \mathbf{r}(u, v)}{\partial v}, \quad (3)$$

where f are hierarchical divergence-conforming basis functions of coordinates u and v , N_u and N_v are the adopted orders of current-approximation, which are entirely independent from the element geometrical orders (K_u and K_v), α_{uj} and α_{vij} are unknown current-distribution coefficients, and $\mathbf{r}(u, v)$ is given in Eq.(1).

In this work, the simple divergence-conforming polynomials were adopted as basis functions [1], given by

$$f_{ij}(u, v) = \begin{cases} u+1, & i=0 \\ u-1, & i=1 \\ u^i-1, & i \geq 2, \text{ even} \\ u^i-u, & i \geq 3, \text{ odd} \end{cases} v^j, \quad (4)$$

with an analogous expression for f_{vij} . Note, however, that other types of hierarchical basis functions can be implemented in the method as well, e.g., the higher-order basis functions with improved orthogonality properties constructed from standard orthogonal polynomials of ultraspherical and Chebyshev type [2] (note that the technique presented in [2] is restricted to bilinear quadrilateral elements only).

3. Numerical Results and Discussion

As the first example, consider the scattering from a metallic sphere of radius $a = 1$ m in the frequency range 10 – 600 MHz. The sphere surface is first approximated using the first-order geometrical modeling ($K_u = K_v = 1$) and second-order current modeling ($N_u = N_v = 2$) in all elements. Shown in Figs.3(a) and 3(b) are the geometrical models constructed from (A) 216 and (B) 600 bilinear quadrilaterals, with the resulting total numbers of unknowns being 1728, and 4800, respectively, without the use of symmetry. Fig.4 shows the radar cross-section (RCS) of the sphere. The results obtained by the higher-order MoM are compared with the analytical solution in the form of Mie's series. An excellent agreement between the numerical results obtained with the model (B) and analytical results is observed in the entire frequency range considered, while the model (A) provides accurate results up to the frequency at which $a/\lambda = 1$. Note that an increase

in the current-approximation orders N_u and N_v in the model (A) does not yield improved accuracy at higher frequencies, meaning that the inaccuracy in the RCS prediction with this model is a consequence of the inaccuracy in geometrical modeling of the sphere surface. Note also that the largest elements in the model (B) are 0.36λ on a side at the highest frequency considered, which is still considerably above the usual small-domain limit of 0.1λ .

The spherical scatterer is next analyzed employing the fourth-order geometrical modeling ($K_u = K_v = 4$ in all elements), with the sphere surface approximated by (C) 6 fourth-order quadrilaterals [Fig.5(a)] in conjunction with the eighth-order current approximation ($N_u = N_v = 8$) in each element and (D) by 24 fourth-order quadrilaterals [Fig.5(b)] with the sixth-order current approximation ($N_u = N_v = 6$) in each element. This results in a total of 768 and 1728 unknowns in models (C) and (D), respectively, with no symmetry used. Shown in Fig.6 is the RCS of the sphere obtained by the two geometrically higher-order MoM models, as compared with the exact solution (Mie's series). We observe an excellent agreement between the numerical results obtained with the model (C) and analytical results up to the frequency at which $a/\lambda = 1.1$ and the curved quadrilateral elements in the model are 1.35λ on a side. With the model (D), an excellent agreement with the exact solution is obtained in the entire frequency range considered.

Consider next a system of wires attached to a metallic cylinder at 833 MHz. The radius of the cylinder is 10 cm and its height 22 cm. The attached wires are an 8-cm driven monopole (radius 1 mm) and 44-cm parasitic monopole (radius 2 mm). Figure 7 shows the simulated geometrical model of the structure with the cylinder being modeled using 32 second-order ($K_u = K_v = 2$) quadrilateral surface elements. Note that triangle-like curved quadrilaterals are used around the wire-to-surface junctions in order to enable the current continuity across junctions. Each monopole is modeled by a single straight wire segment. The results for the radiated far field obtained by the higher-order MoM are compared with the results obtained by the low-order MoM from [3] (Fig.8). The two-fold symmetry is used in both approaches. A very good agreement of the two sets of results is observed, the number of unknowns required by the higher-order MoM (62) being considerably smaller than the number of unknowns required by the low-order MoM [3] (986). Note that the monopole antenna impedance computed by the higher order MoM, $Z_{ant} = (30.0 - j20.9) \Omega$, also agrees very well with the MoM result from [3], $Z_{ant} = (30.0 - j20.2) \Omega$.

References

- [1] B. M. Notaros, B. D. Popovic, J. Peeters Weem, R. A. Brown, and Z. Popovic, "Efficient large-domain MoM solution to electrically large practical EM problems", *IEEE Transactions on Microwave Theory and Techniques*, January 2001, Vol. 49, (1), pp.151-159.
- [2] M. Djordjević and B. M. Notaroš, "Three types of higher-order MoM basis functions automatically satisfying current continuity conditions", *2002 IEEE Antennas and Propagation Society International Symposium Digest*, June 16-21, 2002, San Antonio, TX, U.S.A., pp.IV.610-613.
- [3] R. E. Hodges, and Y. Rahmat-Samii, "An iterative current-based hybrid method for complex structures", *IEEE Transactions on Antennas and Propagation*, Vol.45, No.2, February 1997, pp.265-276.

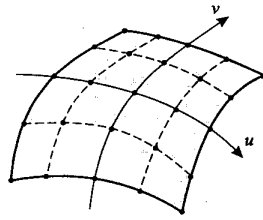


Fig.1. Generalized curved quadrilateral.

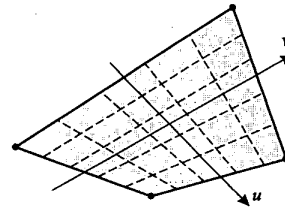


Fig.2. Bilinear quadrilateral.

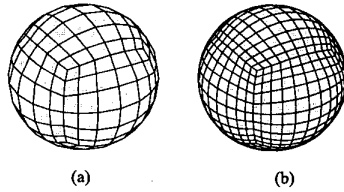


Fig.3. Spherical scatterer modeled using (a) 216 and (b) 600 bilinear quadrilaterals.

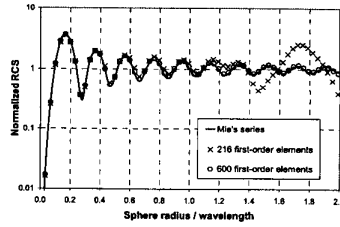


Fig.4. Calculated RCS of the metallic sphere using two models in Fig.3.

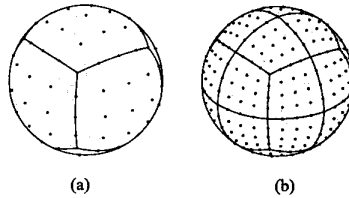


Fig.5. Spherical scatterer modeled by (a) 6 and (b) 24 fourth-order quadrilaterals.

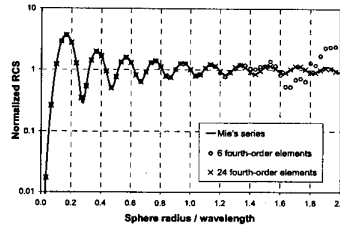


Fig.6. Calculated RCS of the metallic sphere using two models in Fig.5.

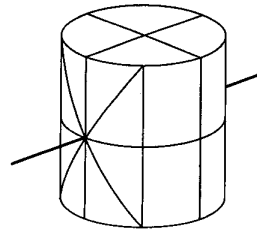


Fig.7. An antenna system modeled by 32 second-order quadrilaterals and two wires.

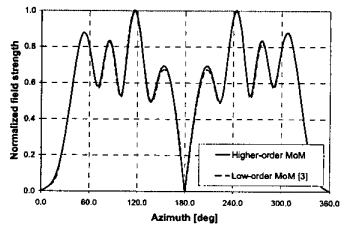


Fig.8. Normalized far field pattern of the antenna system in Fig.7.